

# Vortex and soliton dynamics in particle-hole symmetric superfluids

Jim Skulte,<sup>1,2</sup> Lukas Broers,<sup>1</sup> Jayson G. Cosme,<sup>3</sup> and Ludwig Mathey<sup>1,2</sup>

<sup>1</sup>Zentrum für Optische Quantentechnologien and Institut für Laserphysik, Universität Hamburg, 22761 Hamburg, Germany

<sup>2</sup>The Hamburg Centre for Ultrafast Imaging, Luruper Chaussee 149, 22761 Hamburg, Germany

<sup>3</sup>National Institute of Physics, University of the Philippines, Diliman, Quezon City 1101, Philippines

(Dated: November 16, 2021)

We propose to induce topological defects in particle-hole symmetric superfluids, with the prime example of the BCS state of ultracold atoms and detect their time evolution and decay. We demonstrate that the time evolution is qualitatively distinct for particle-hole symmetric superfluids, and point out that the dynamics of topological defects is strongly modified in particle-hole symmetric fluids. We obtain results for different charges and compare them with the standard Gross-Pitaevskii prediction for Bose-Einstein condensates. We highlight the observable signatures of the particle-hole symmetry in the dynamics of decaying solitons and subsequent vortices.

The presence or absence of particle-hole symmetry in a physical system is a fundamental property pervading its dynamical properties. Particle-hole symmetry is realised in Lorentz invariant theories such as the standard model of elementary physics [1], low energy effective models close to quantum criticality [2], and the famous Bardeen-Cooper-Schrieffer (BCS) theory of superconductivity [3, 4], note [5]. We note that the order parameter dynamics of high- $T_c$  superconductors can be described by an effective particle-hole symmetric theory, which allows for exploring the dynamics of the Higgs/amplitude mode [6–9]. Similarly, in ultracold neutral atoms the emergence of an effective particle-hole symmetry has been theoretically predicted [10, 11] and confirmed experimentally [12, 13]. Recently, amplitude oscillations of the order parameter in the BEC-BCS crossover have been reported [14], suggesting the presence of approximate particle-hole symmetry.

The dynamics of topological defects, such as solitons and quantized vortices, derives from and exemplifies the properties of the underlying quantum fluid. The stability of solitons has been discussed extensively for the nonlinear Schrödinger equation or Gross-Pitaevskii equation (GP) [15–19]. Zakharov and Rubenchik coined the term ‘snaking’ to refer to the characteristic bending of solitons prior to their decay. Snaking is a manifestation of the Magnus force. This has been discussed for neutral bosonic systems within the GP equation [20–26], in the BEC-BCS crossover [27–29], as well as in superconductors [30, 31].

We propose to determine the influence of particle-hole symmetry on the dynamics of topological defects in two-dimensional (2D) neutral superfluids. We focus on the BCS state as our primary example, but our results hold for any approximately particle-hole symmetric system, e.g. bosons in an optical lattice near unit filling [13]. For this purpose we present the similarities and differences in the dynamics of topological defects in the absence and presence of particle-hole symmetry. We also compare the dynamics of the particle-hole symmetric theory for zero and nonzero Noether charge, corresponding to a balanced

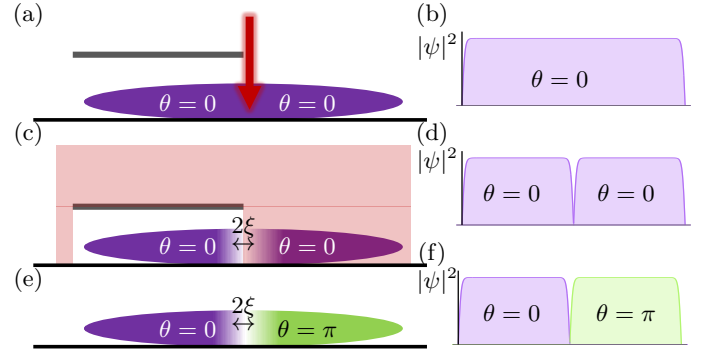


FIG. 1. Schematic representation of the proposed protocol to imprint a soliton in (a),(c),(e) and the corresponding density profiles  $|\psi|^2$  and phase distributions  $\theta$  in (b),(d),(f). A narrow laser sheet is applied to a quantum fluid on the BEC side of the crossover to create a density depletion in the condensate (a). The quantum fluid is split into two subsystems with a relative phase of zero, see (b) and (d). Next, a  $\pi$ -pulse is applied to half of the condensate (c) to create the phase pattern of a dark soliton, see (e) and (f). Next, the interaction is adiabatically changed across the crossover deep into the BCS side. The narrow laser sheet separating the two subsystems is removed, which triggers the soliton dynamics.  $\xi$  is the healing length of the condensate.

mixture of particles and holes and an imbalanced mixture of particles and holes, respectively. We find that the case with nonzero charge is reminiscent of the dynamics of the GP equation. On the other hand, for vanishing charge, in which the number of particles and holes is balanced, we show that vortices do not experience any Magnus force. This leads to a soliton decay without snaking, setting it apart from soliton dynamics in non-particle-hole symmetric fluids, such as BECs. To induce soliton dynamics of the quantum fluid in the BCS limit, we propose to imprint a soliton on the BEC side of the crossover in the presence of a potential barrier. As a next step, we propose to ramp the fluid adiabatically across the crossover into the BCS limit, while keeping the barrier potential

up. Finally, the barrier potential is ramped to zero, to induce the soliton dynamics. This protocol of initializing the dynamics enables imprinting of the phase pattern with an off-resonant optical pulse, whereas direct phase imprinting in the particle-hole symmetric limit is prohibited. We note that this statement holds only for an exact particle-hole symmetric case. In experiments such as those in Ref. [28], particle-hole symmetry is only approximately realised. That is, the appropriate effective action is expected to have both  $K_1\partial_t$  and  $K_2\partial_t^2$  contributions, as we discuss below. The  $K_1\partial_t$  term allows the phase imprinting as it is the dominant term in the BEC regime. The proposed protocol is displayed in Fig 1.

We consider a low-energy effective models of the form [3]

$$\mathcal{S} = \int d^2x dt \left\{ K_2 (\partial_t \psi) (\partial_t \bar{\psi}) - iK_1 (\partial_t \psi) \bar{\psi} - \frac{1}{m} \nabla \bar{\psi} \nabla \psi - \mu |\psi|^2 + \frac{g}{2} |\psi|^4 + V_{\text{ext}} |\psi|^2 - i\mu_Q ((\partial_t \bar{\psi}) \psi - \bar{\psi} \partial_t \psi) \right\}, \quad (1)$$

where  $K_{1,2}$  are the above-mentioned parameters that determine the time dependence,  $\mu$  is the square root of the gap energy, which has the dimensions of a mass term,  $g$  is the contact interaction strength and  $V_{\text{ext}}$  is the externally applied potential. A similar effective field theory has been proposed and discussed to model the BEC-BCS crossover in [32–35]. We include a Lagrange multiplier  $\mu_Q$  to fix the Klein-Gordon charge (7), see below. By setting  $K_2 = 0$  and  $K_1 = 1$  and  $\mu_Q = 0$ , we recover the GP equation

$$i\partial_t \psi(\mathbf{x}, t) = \frac{\nabla^2}{2m} \psi(\mathbf{x}, t) + V(|\psi|^2) \psi(\mathbf{x}, t), \quad (2)$$

where  $V(|\psi(\mathbf{x}, t)|^2) = \mu - g|\psi(\mathbf{x}, t)|^2 + V_{\text{ext}}(\mathbf{x})$ . We refer to a condensate described by the GP equation as a GP fluid. This equation is manifestly not particle-hole symmetric under the exchange  $\psi \leftrightarrow \bar{\psi}$ . On the other hand, particle-hole symmetry is fulfilled in the action (1) by setting  $K_1 = 0$  and  $K_2 \neq 0$ . We introduce a dimensionless representation via  $\psi = \tilde{\psi}/\xi$ ,  $\nabla = \tilde{\nabla}/\xi$ ,  $\partial_t = c_s/\xi \tilde{\partial}_t$  and  $V = \mu \tilde{V}$ , where  $\xi$  is the healing length of the fluid and  $c_s$  the speed of sound. This leads to the modified nonlinear Klein-Gordon (NLKG) equation

$$\partial_t^2 \tilde{\psi}(\mathbf{x}, t) = \tilde{\nabla}^2 \tilde{\psi}(\mathbf{x}, t) + \tilde{V}(|\tilde{\psi}|^2) \tilde{\psi}(\mathbf{x}, t) + i\mu_Q \partial_t \tilde{\psi}(\mathbf{x}, t). \quad (3)$$

We refer to condensates evolving according to the NLKG equation as Klein-Gordon (KG) fluids. In the following we drop the tilde. We trap the fluid using a box potential of the form

$$V_{\text{ext}}(\mathbf{x}) = V_0 (1 + \tanh((|\mathbf{x}| - r_0)/\xi)). \quad (4)$$

We note that this model is a relativistic BEC [36–38] and a similar equation has been proposed to model cold dark

matter [39–41] and relativistic boson stars [42–44].

In the following, we show the influence of particle-hole symmetry on the dynamics of topological defects. For the KG fluid, we introduce the canonical momentum  $\Pi(x, t) = \partial_t \bar{\psi}(x, t) + i\mu_Q \bar{\psi}(x, t)$  to obtain two coupled first order partial differential equations

$$\begin{aligned} \partial_t \psi(\mathbf{x}, t) &= \bar{\Pi}(\mathbf{x}, t) + i\mu_Q \psi(\mathbf{x}, t), \\ \partial_t \Pi(\mathbf{x}, t) &= \nabla^2 \bar{\psi}(\mathbf{x}, t) + V(|\psi|^2) \bar{\psi}(\mathbf{x}, t) - i\mu_Q \Pi(\mathbf{x}, t). \end{aligned} \quad (5)$$

A crucial feature of a KG fluid is that the particle number  $N = \int |\psi(\mathbf{x}, t)|^2 dx$  is not conserved, in contrast to a GP fluid. Instead, in the KG fluid, the Noether charge

$$Q = -i \int (\bar{\Pi}(\mathbf{x}, t) \bar{\psi}(\mathbf{x}, t) - \Pi(\mathbf{x}, t) \psi(\mathbf{x}, t)) d^2x \quad (7)$$

is conserved. The Noether charge  $Q$  can be thought of as the difference of particles and holes in the system. That is, a zero Noether charge describes the situation with an equal number of particles and holes. An intuitive example for illustrating the Noether charge is a system of interacting bosons in an optical lattice with unit filling. An excitation corresponds to exciting one atom out of the lattice site and leaving behind a hole. Thus, the Noether

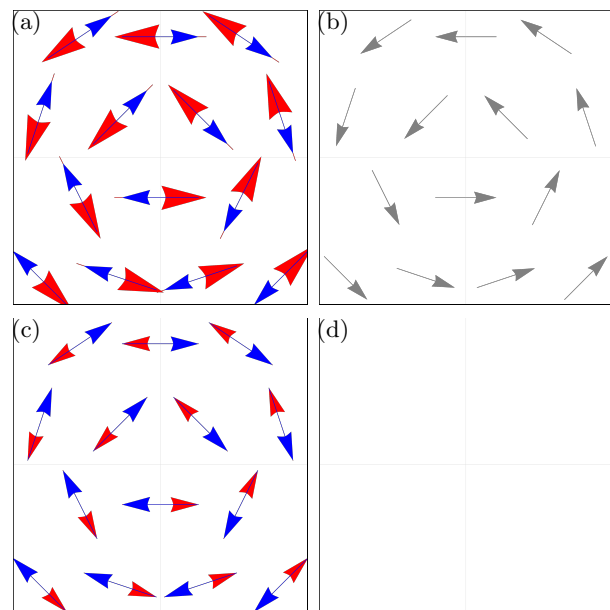


FIG. 2. Schematic sketch of the local velocity fields of the particles (blue) and antiparticles (red) in (a) and (c) and the resulting total local velocity field for the  $\psi$  field (gray) in (b) and (d). A unbalanced mixture of particles and antiparticles with a finite charge  $Q$  (a) leads to a non-zero effective velocity field for the  $\psi$  field (b). A balanced mixture of particles and antiparticles with a vanishing charge  $Q$  (c) leads to a vanishing effective velocity field for the  $\psi$  field (d)

charge stays unchanged as the same number of particles and hole were created. Another possible excitation is to excite the atom out of the lattice and further removing it from the system, which leaves a hole behind. The system then slightly goes away from unit filling as there is now an imbalance between the number of holes and particles and this corresponds to an effective nonzero Noether charge. Another example can be envisioned in the BCS regime for nonzero temperature. Here, a RF "knife" can be used to remove some of the atoms occupying the Bogoliubov modes leading to an imbalance between particle and hole excitations.

We apply the Madelung transformation to the field and the canonical momentum, in which the field  $\psi$  is written in an amplitude-phase representation:

$$\psi(\mathbf{x}, t) = A(\mathbf{x}, t) \exp(i\theta(\mathbf{x}, t)) \quad (8)$$

$$\Pi(\mathbf{x}, t) = \left( \frac{\dot{A}(\mathbf{x}, t)}{A(\mathbf{x}, t)} + i [\mu_Q - \dot{\theta}(\mathbf{x}, t)] \right) \psi(\mathbf{x}, t) \quad (9)$$

and obtain the continuity equation and particle-hole symmetric Euler equation

$$\partial_t \rho_{\text{KG}} + \frac{\mu_Q}{2} \partial_t \rho_S = -\nabla \cdot (\rho_S \mathbf{u}), \quad (10)$$

$$\left( \frac{\rho_{\text{KG}}}{\rho_S} + \frac{\mu_Q}{2} \right) \partial_t \mathbf{u} = \mathbf{u} \nabla \mathbf{u} + \frac{\nabla \rho_S}{2\rho_0} - \frac{\nabla}{2} \left( \frac{\square \sqrt{\rho_S}}{\sqrt{\rho_S}} \right), \quad (11)$$

where we introduce the GP density  $\rho_S = A^2$ , the KG density  $\rho_{\text{KG}} = A^2 \partial_t \theta$ , the velocity  $\mathbf{u} = \nabla \theta$ , and the box operator  $\square = \partial_t^2 - \nabla^2$ . In this representation, the charge simplifies to  $Q = \int \rho_{\text{KG}} dx$ . In the particle-hole symmetric Euler equations there is a prefactor  $\rho_{\text{KG}}/\rho_S$  in front of the time derivative of the velocity field  $\partial_t \mathbf{u}$ . This prefactor depends on the charge  $Q$ . This is a crucial difference to the GP Euler equation where this prefactor is always 1.

The particle-hole symmetric Euler equation, Eq. (11), has two quantum pressure terms. One term is due to the kinetic energy of the condensate, and is proportional to  $\frac{\nabla^2 \sqrt{\rho_S}}{\sqrt{\rho_S}}$ . It is the zero point motion of the condensate and becomes dominant if the condensate has spatial variations on short length scales [45]. The second is proportional to  $\frac{\partial_t^2 \sqrt{\rho_S}}{\sqrt{\rho_S}}$  and originates from the second-order time derivative. It only exists for particle-hole symmetric condensates.

We present the local velocity field around a single vortex. Therefore we transform into the Feshbach-Villars basis, which translates the NLKG to coupled GP equations for the particles and antiparticles, respectively [46]

$$\psi = \frac{1}{\sqrt{2}} (\psi^{\text{P}} + \psi^{\text{a}}), \quad (12)$$

$$\Pi = \frac{i}{\sqrt{2}} (\psi^{\text{a}} - \psi^{\text{P}}). \quad (13)$$

Next, we expand the field around the vortex core position  $r_0$  with the amplitude  $A^i$  and phase  $\theta^i$  (see Eq. 8,9) and propagate the location of the vortex core using the equations of motion and compare the new location to the previous location to obtain the local velocity field. See for a detailed discussion and derivation [47–49]. For the two velocity fields we obtain

$$v^{\text{a}} = - \frac{(-i, 1)^{\text{T}} \cdot \vec{\nabla} (A^{\text{P}} + A^{\text{a}}) + (A^{\text{P}} + A^{\text{a}}) (1, i)^{\text{T}} \cdot \vec{\nabla} \theta}{A^{\text{a}}}, \quad (14)$$

$$v^{\text{P}} = \frac{(-i, 1)^{\text{T}} \cdot \vec{\nabla} (A^{\text{P}} + A^{\text{a}}) + (A^{\text{P}} + A^{\text{a}}) (1, i)^{\text{T}} \cdot \vec{\nabla} \theta}{A^{\text{P}}}, \quad (15)$$

where the spatial plane  $(x, y)$  is represented as the complex plane  $z = x + iy$ . Translating this back into the

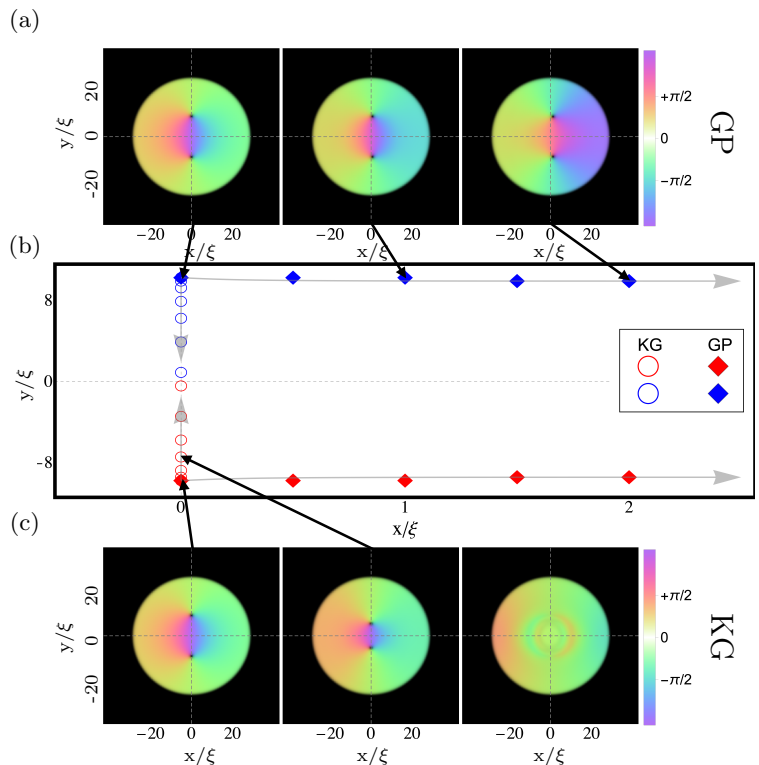


FIG. 3. Dynamics of vortex dipole pairs in a GP and KG fluid. (a) and (c) display the phase and the density of the GP fluid (a), and the KG fluid (c). (b) The circles display the location of the vortices and anti-vortices in red and blue, respectively, of the GP fluid (diamonds) and the KG fluid (circles), and difference times. The snapshots of (a) and (c) are indicated via black arrows. The gray arrows indicate the movement of the vortices in time.

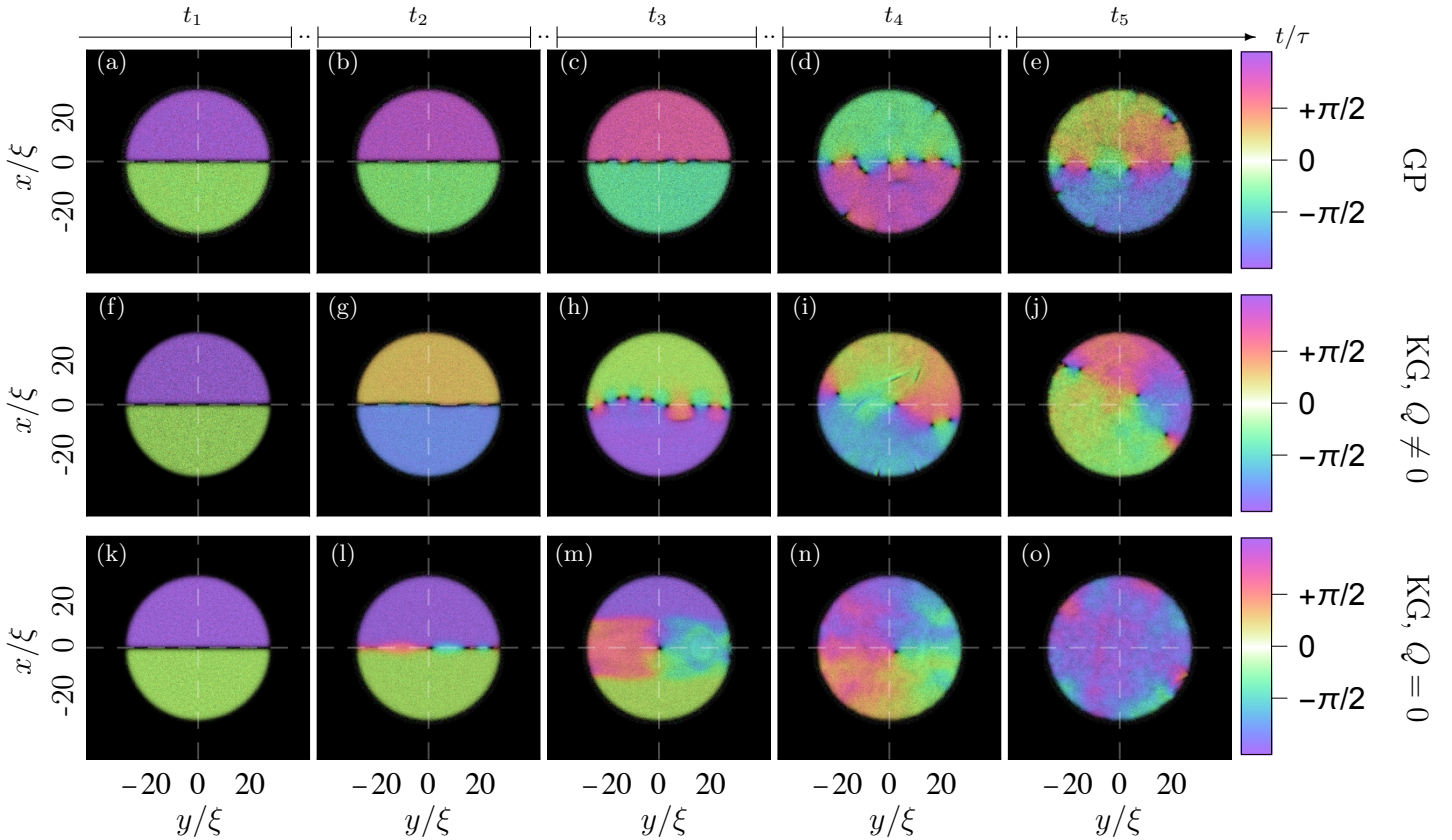


FIG. 4. Overview of the soliton instability for the three distinct cases corresponding to GP (a)-(e), KG with  $Q \neq 0$  (f)-(j) and KG with  $Q = 0$  (k)-(o). For better comparison between GP and KG the  $\psi$  field density is normalised such that the maximum value is set to unity in each snapshot. The shading of the plots ranging from black to white visualises the magnitude of the field  $|\psi|$ , while the colormap indicates the phase. (a),(f),(k) Initial soliton seeded with white noise. (b),(g),(l) Soliton bending. (c),(h),(m) Vortices appearing after the soliton decay. The long-time dynamics of the vortices inside the trap are presented in (d),(i),(n) and (e),(j),(o). White dashed lines indicate the soliton axis and the perpendicular axis. The spatial length is expressed in terms of the healing length  $\xi$ . A movie showing this dynamics is presented in the supplemental material [49].

( $\psi, \Pi$ ) basis we obtain

$$v^\psi = \frac{1}{\sqrt{2}} (v^p + v^a) = \sqrt{2} \left( 1 - \frac{A^a}{A^p} \right) v^p. \quad (16)$$

For  $Q \neq 0$  we have  $A^a \neq A^p$ , which means that we obtain a non-zero velocity field. In this case the velocity is proportional to the velocity obtained for GP fluids [48]. For  $Q = 0$ , we have  $A^p = A^a$  and  $N^p = N^a$  with  $N^i$  the total number of particles/antiparticles. For this balanced scenario the local velocity field vanishes precisely as shown in Fig. 2. As pointed out before and as can be seen from Eq. (16), for a finite charge  $Q$  corresponding to an imbalance between particles and antiparticles the magnitudes of the velocity fields are different, see Fig. 2(a), which results in a non-zero velocity field for the KG fluid  $\psi$  (see Fig. 2(b)). In contrast, for a balanced mixture the local velocity fields magnitudes are the same (see Fig. 2(c)) and due to the opposite direction of the velocity fields the velocity field of the KG fluid vanishes (see Fig. 2(d)). To expand on our analytical predictions

and to propose an experimental setup to detect vortex dynamics of KG fluids, we simulate the equations using the pseudo-spectral method [50] for both the GP and KG fluids. We set the ratio between the chemical potential  $\mu$  and the contact interaction  $g$  to  $\mu/g = 10/\xi^2$ . In the following we express all length scales in units of  $\xi$ . Our simulations are discretized in a  $256 \times 256$  grid. We choose  $r_0/\xi = 25$ , where  $r_0$  is half of the box size, as defined in Eq. 4 and resolve  $\xi$  with 3 grid points. The phase and density distribution for snapshots in real time are shown for a GP fluid (see Fig. 3(a)) and for a KG fluid with vanishing charge (see Fig. 3(c)). Circles (KG fluid with  $Q = 0$ ) and diamonds (GP fluid) in red correspond to a phase winding of  $+1$ , while blue corresponds to  $-1$  (see Fig. 3(b)). The gray arrows show the flow of time in the figure. It can be seen that for a dipole distance  $d_{12} > 2\xi$  in the GP fluid the dipole will start to propel forwards perpendicular to the dipole axis and will not annihilate. In contrast, the KG vortex dipole will move along the dipole axis and annihilate each other, due to

the absence of a velocity field. Related observations of vortex dynamics were reported in [51]. We note that the particle-hole symmetry is the origin of this qualitatively distinct behaviour from GP fluid dynamics. We propose that the data from a future experimental realization of our proposal could be used to numerically fit the ratio of  $K_1$  and  $K_2$  for different interaction strengths. This links our proposal to the parameters used in the universal effective action of such systems.

To investigate the influence of the particle-hole symmetry on the soliton dynamics, we initialise the condensate with a modified Thomas-Fermi profile [45], as described in the supplemental material [49], for a box potential in Eq. (4) with  $V_0 = 10$  and  $r_0 = 30$  for the GP (KG) fluid and start with a soliton imprinted in the fluid. We let the condensate relax using the imaginary time propagation [52] extended to particle-hole symmetric fluids [49]. For the KG fluids, we set the initial canonical momentum as  $\Pi = i\frac{\mu_Q}{2}\psi$  with  $\mu_Q \in \mathbb{R}$ , resulting in a charge of  $Q = \mu_Q N$ . Furthermore, we add 1% white noise on the initial condensate density to study the stability of solitons.

The system is propagated in time according to Eqs. (2), (5) and (6). At lowest order, the Higgs mode and the Goldstone mode decouple in a particle-hole symmetric theory [3]. Within this approximation, this initial state only induces dynamics of the Goldstone mode. However, this approximation fails in soliton and vortex solutions. For the same parameters  $\mu$  and  $g$ , the healing length is twice as large in the KG case compared to GPE due to the difference in the prefactor of the kinetic energy.

In Fig. 4, we present the real time dynamics of the complex field  $\psi$  shaded from white to black corresponding to decreasing amplitude, i.e. black regions denote areas with vanishing  $|\psi|$ . The phase of the wave function is represented as color. The wave function is normalised for each snapshot such that the maximum value is set to unity to make it easier to compare GP and KG results.

In the GP fluid, we observe the established soliton instability in Figs. 4(a)-4(c) [17] and the motion of trapped vortices in Figs. 4(c)-4(e) [24, 48]. The vortices move towards the edge of the condensate. As they approach the edge, they experience a net force and move along the trap boundary as depicted in Figs. 4(d) and 4(e) [24]. The behaviour of the KG fluid with  $Q \neq 0$  is similar. As displayed in Figs. 4(f)-4(j), the soliton decays into vortices, which then move around the condensate. Similar to the GP fluid, as the phase rotates in Figs. 4(f)-4(j), the vortices experience a net force leading to their motion along the trap boundary as seen in Figs. 4(i)-4(j).

In contrast, for the KG fluid with  $Q = 0$ , the soliton decays into vortices that are located along the soliton axis, as shown in Figs. 4(k)-4(m). Similar results have been found in [29]. Moreover, we find that the vortices are not rotating as displayed in Figs. 4(m)-4(o), which is consistent with Eqs. (14), (16) and Fig. 3. When the

vortices reach the trap boundary, they evaporate into the thermal cloud as shown in Figs. 4(n) and 4(o).

In conclusion, we have shown that by measuring the density profile of a 2D condensate after imprinting a soliton in a particle-hole symmetric superfluid, such as a BCS state of neutral particles, it is possible to test the effective low-energy theoretical description of the system. We have shown analytically and numerically that for particle-hole symmetric superfluids with vanishing Noether charge the Magnus force is absent. This allows for a dipole pair of vortices to approach each other without transverse motion and to annihilate, reminiscent of recent observation in [51]. Another consequence of the vanishing Magnus force is that a soliton does not bend as it decays into vortices. Probing these effects experimentally will reveal how well particle-hole symmetry is realised in the dynamics of superfluids or whether the non-particle-hole symmetric term, the first-order derivative in time, is the dominant contribution in the effective theory. This is crucial in understanding the notion of turbulence in particle-hole symmetric fluids such as superconductors. Our work reveals that turbulence in a BCS superconductor and its scaling laws might deviate from Kolmogorow scaling laws [53], which apply to classical systems as well to GP fluids. We note that our predictions could be experimentally confirmed using refined experimental technique, such as *in situ* observations of two dimensional Fermi liquids when probing the BEC-BCS crossover in neutral atoms [54, 55] or the well controlled imprinting of vortex dipole pairs [51].

We thank Guido Homann and Antonio Muñoz Mateo for fruitful discussions. This work is supported by the Deutsche Forschungsgemeinschaft (DFG) in the framework of SFB 925, Project No. 170620586, and the Cluster of Excellence ‘‘Advanced Imaging of Matter’’ (EXC 2056), Project No. 390715994. J.S. acknowledges support from the German Academic Scholarship Foundation.

- 
- [1] S. Weinberg, *The quantum theory of fields. Vol. 2: Modern applications* (Cambridge University Press, 2013).
  - [2] S. Sachdev, *Quantum Phase Transitions*, 2nd ed. (Cambridge University Press, 2011).
  - [3] D. Pekker and C. Varma, Amplitude/Higgs Modes in Condensed Matter Physics, *Annual Review of Condensed Matter Physics* **6**, 269–297 (2015).
  - [4] C. M. Varma, Higgs Boson in Superconductors, *Journal of Low Temperature Physics* **126**, 901 (2002).
  - [5] Due to the close connection between relativistic Lorentz invariance and particle-hole symmetry, models that are particle-hole symmetric are also sometimes referred to as relativistic models.
  - [6] G. Homann, J. G. Cosme, and L. Mathey, Higgs time crystal in a high- $T_c$  superconductor, *Phys. Rev. Research* **2**, 043214 (2020).
  - [7] G. Homann, J. G. Cosme, J. Okamoto, and L. Mathey,

- Higgs mode mediated enhancement of interlayer transport in high- $T_c$  cuprate superconductors, *Phys. Rev. B* **103**, 224503 (2021).
- [8] Z. Dai and P. A. Lee, Photo-induced superconducting-like response in strongly correlated systems (2021), [arXiv:2103.09255](https://arxiv.org/abs/2103.09255) [cond-mat.str-el].
- [9] Z. Dai and P. A. Lee, Superconducting-like response in driven systems near the mott transition (2021), [arXiv:2106.08354](https://arxiv.org/abs/2106.08354) [cond-mat.str-el].
- [10] E. Altman and A. Auerbach, Oscillating superfluidity of bosons in optical lattices, *Physical Review Letters* **89**, 10.1103/physrevlett.89.250404 (2002).
- [11] L. Pollet and N. Prokof'ev, Higgs mode in a two-dimensional superfluid, *Physical Review Letters* **109**, 10.1103/physrevlett.109.010401 (2012).
- [12] J. Léonard, A. Morales, P. Zupancic, T. Donner, and T. Esslinger, Monitoring and manipulating Higgs and Goldstone modes in a supersolid quantum gas, *Science* **358**, 1415–1418 (2017).
- [13] M. Endres, T. Fukuhara, D. Pekker, M. Cheneau, P. Schauss, C. Gross, E. Demler, S. Kuhr, and I. Bloch, The "Higgs" amplitude mode at the two-dimensional superfluid/Mott insulator transition, *Nature* **487**, 454–458 (2012).
- [14] A. Behrle, T. Harrison, J. Kombe, K. Gao, M. Link, J. S. Bernier, C. Kollath, and M. Köhl, Higgs mode in a strongly interacting fermionic superfluid, *Nature Physics* **14**, 781 (2018).
- [15] V. E. Zakharov and A. M. Rubenchik, Instability of waveguides and solitons in nonlinear media, *Soviet Journal of Experimental and Theoretical Physics* **38**, 494 (1974).
- [16] C. A. Jones, S. J. Putterman, and P. H. Roberts, Motions in a Bose condensate. V. Stability of solitary wave solutions of non-linear Schrodinger equations in two and three dimensions, *Journal of Physics A: Mathematical and General* **19**, 2991 (1986).
- [17] J. Brand and W. P. Reinhardt, Solitonic vortices and the fundamental modes of the "snake instability": Possibility of observation in the gaseous Bose-Einstein condensate, *Phys. Rev. A* **65**, 043612 (2002).
- [18] A. Muñoz Mateo and J. Brand, Chladni Solitons and the Onset of the Snaking Instability for Dark Solitons in Confined Superfluids, *Phys. Rev. Lett.* **113**, 255302 (2014).
- [19] P. G. Kevrekidis, I. Danaïla, J.-G. Caputo, and R. Carretero-González, Planar and radial kinks in non-linear Klein-Gordon models: Existence, stability, and dynamics, *Phys. Rev. E* **98**, 052217 (2018).
- [20] N.-E. Guenther, P. Massignan, and A. L. Fetter, Quantized superfluid vortex dynamics on cylindrical surfaces and planar annuli, *Phys. Rev. A* **96**, 063608 (2017).
- [21] L. A. Toikka and J. Brand, Asymptotically solvable model for a solitonic vortex in a compressible superfluid, *New Journal of Physics* **19**, 023029 (2017).
- [22] B. Jackson, J. F. McCann, and C. S. Adams, Vortex line and ring dynamics in trapped Bose-Einstein condensates, *Phys. Rev. A* **61**, 013604 (1999).
- [23] S. A. McGee and M. J. Holland, Rotational dynamics of vortices in confined Bose-Einstein condensates, *Phys. Rev. A* **63**, 043608 (2001).
- [24] D. E. Sheehy and L. Radzihovsky, Vortices in spatially inhomogeneous superfluids, *Phys. Rev. A* **70**, 063620 (2004).
- [25] J. Denschlag, J. E. Simsarian, D. L. Feder, C. W. Clark, L. A. Collins, J. Cubizolles, L. Deng, E. W. Hagley, K. Helmerson, W. P. Reinhardt, S. L. Rolston, B. I. Schneider, and W. D. Phillips, Generating solitons by phase engineering of a bose-einstein condensate, *Science* **287**, 97 (2000), <https://science.sciencemag.org/content/287/5450/97.full.pdf>.
- [26] S. Burger, K. Bongs, S. Dettmer, W. Ertmer, K. Senstock, A. Sanpera, G. V. Shlyapnikov, and M. Lewenstein, Dark solitons in bose-einstein condensates, *Phys. Rev. Lett.* **83**, 5198 (1999).
- [27] M. W. Zwierlein, J. R. Abo-Shaeer, A. Schirotzek, C. H. Schunck, and W. Ketterle, Vortices and superfluidity in a strongly interacting fermi gas, *Nature* **435**, 1047 (2005).
- [28] M. J. H. Ku, W. Ji, B. Mukherjee, E. Guardado-Sanchez, L. W. Cheuk, T. Yefsah, and M. W. Zwierlein, Motion of a Solitonic Vortex in the BEC-BCS Crossover, *Phys. Rev. Lett.* **113**, 065301 (2014).
- [29] W. Van Alphen, H. Takeuchi, and J. Tempere, Crossover between snake instability and josephson instability of dark solitons in superfluid fermi gases, *Phys. Rev. A* **100**, 023628 (2019).
- [30] J. Bardeen and M. J. Stephen, Theory of the Motion of Vortices in Superconductors, *Phys. Rev.* **140**, A1197 (1965).
- [31] P. Ao and D. J. Thouless, Berry's phase and the Magnus force for a vortex line in a superconductor, *Phys. Rev. Lett.* **70**, 2158 (1993).
- [32] S. N. Klimin, J. Tempere, and J. T. Devreese, Finite-temperature effective field theory for dark solitons in superfluid fermi gases, *Phys. Rev. A* **90**, 053613 (2014).
- [33] S. N. Klimin, J. Tempere, G. Lombardi, and J. T. Devreese, Finite temperature effective field theory and two-band superfluidity in fermi gases, *The European Physical Journal B* **88**, 122 (2015).
- [34] G. Lombardi, W. Van Alphen, S. N. Klimin, and J. Tempere, Soliton-core filling in superfluid fermi gases with spin imbalance, *Phys. Rev. A* **93**, 013614 (2016).
- [35] W. V. Alphen, G. Lombardi, S. N. Klimin, and J. Tempere, Dark soliton collisions in superfluid fermi gases, *New Journal of Physics* **20**, 053052 (2018).
- [36] S. Fagnocchi, S. Finazzi, S. Liberati, M. Kormos, and A. Trombettoni, Relativistic Bose-Einstein condensates: a new system for analogue models of gravity, *New Journal of Physics* **12**, 095012 (2010).
- [37] H. E. Haber and H. A. Weldon, Thermodynamics of an Ultrarelativistic Ideal Bose Gas, *Phys. Rev. Lett.* **46**, 1497 (1981).
- [38] M. Grether, M. de Llano, and G. A. Baker, Bose-Einstein Condensation in the Relativistic Ideal Bose Gas, *Phys. Rev. Lett.* **99**, 200406 (2007).
- [39] K. Huang, H.-B. Low, and R.-S. Tung, Scalar Field Cosmology II: Superfluidity, Quantum Turbulence, and Inflation, *International Journal of Modern Physics A* **27**, 1250154 (2012).
- [40] J. Magaña, T. Matos, A. Suárez, and F. Sánchez-Salcedo, Structure formation with scalar field dark matter: the field approach, *Journal of Cosmology and Astroparticle Physics* **2012** (10), 003–003.
- [41] C. Xiong, M. R. Good, Y. Guo, X. Liu, and K. Huang, Relativistic superfluidity and vorticity from the non-linear Klein-Gordon equation, *Physical Review D* **90**, 10.1103/physrevd.90.125019 (2014).
- [42] M. Colpi, S. L. Shapiro, and I. Wasserman, Boson Stars:

- Gravitational Equilibria of Self-Interacting Scalar Fields, *Phys. Rev. Lett.* **57**, 2485 (1986).
- [43] P.-H. Chavanis and T. Harko, Bose-Einstein condensate general relativistic stars, *Physical Review D* **86**, 10.1103/physrevd.86.064011 (2012).
- [44] A. Suárez and P.-H. Chavanis, Hydrodynamic representation of the Klein-Gordon-Einstein equations in the weak field limit: General formalism and perturbations analysis, *Physical Review D* **92**, 10.1103/physrevd.92.023510 (2015).
- [45] C. J. Pethick and H. Smith, *Bose-Einstein Condensation in Dilute Gases*, 2nd ed. (Cambridge University Press, 2008).
- [46] H. Feshbach and F. Villars, Elementary relativistic wave mechanics of spin 0 and spin 1/2 particles, *Rev. Mod. Phys.* **30**, 24 (1958).
- [47] O. Törnkvist and E. Schröder, Vortex Dynamics in Dissipative Systems, *Physical Review Letters* **78**, 1908–1911 (1997).
- [48] A. J. Groszek, D. M. Paganin, K. Helmerson, and T. P. Simula, Motion of vortices in inhomogeneous Bose-Einstein condensates, *Phys. Rev. A* **97**, 023617 (2018).
- [49] See supplemental material, .
- [50] W. Bao, D. Jaksch, and P. A. Markowich, Numerical solution of the Gross-Pitaevskii equation for Bose-Einstein condensation, *Journal of Computational Physics* **187**, 318–342 (2003).
- [51] W. J. Kwon, G. D. Pace, K. Khani, L. Galantucci, A. M. Falconi, M. Inguscio, F. Scazza, and G. Roati, Sound emission and annihilations in a programmable quantum vortex collider (2021), [arXiv:2105.15180](https://arxiv.org/abs/2105.15180) [cond-mat.quant-gas].
- [52] C. Barenghi and N. G. Parker, *A Primer on Quantum Fluids*, SpringerBriefs in Physics 10.1007/978-3-319-42476-7 (2016).
- [53] A. Kolmogorov, The Local Structure of Turbulence in Incompressible Viscous Fluid for Very Large Reynolds' Numbers, *Akademiia Nauk SSSR Doklady* **30**, 301 (1941).
- [54] K. Hueck, N. Luick, L. Sobirey, J. Siegl, T. Lompe, and H. Moritz, Two-Dimensional Homogeneous Fermi Gases, *Phys. Rev. Lett.* **120**, 060402 (2018).
- [55] L. Sobirey, N. Luick, M. Bohlen, H. Biss, H. Moritz, and T. Lompe, Observation of superfluidity in a strongly correlated two-dimensional Fermi gas (2020), [arXiv:2005.07607](https://arxiv.org/abs/2005.07607) [cond-mat.quant-gas].